

Non-interacting central site model: localization and logarithmic entanglement growth

Daniel Hetterich¹, Maksym Serbyn², Fernando Domínguez¹, Frank Pollmann³, and Björn Trauzettel¹

¹*Institut für Theoretische Physik, Universität Würzburg, D-97074 Würzburg, Germany*

²*Department of Physics, University of California, Berkeley, California 94720, USA and*

³*Max-Planck Institute for the Physics of Complex Systems, D-0118 Dresden, Germany*

(Dated: January 12, 2017)

We investigate the stationary and dynamical behavior of an Anderson localized chain coupled to a single central bound state. The coupling to the central site partially dilutes the Anderson localized peak towards the nearly resonant sites. In particular, the number of resonantly coupled sites remains finite in the thermodynamic limit. This is further supported by a multifractal analysis of eigenstates that shows the frozen spectrum of fractal dimension, which is characteristic for localized phases in models with power-law hopping. Although the well-known Fano-resonance problem is seemingly similar to our system, it fails to describe it because of the absence of level repulsion within the energy spectrum. For weak coupling strengths to the central site, we identify a regime with a logarithmic in time transport of particles and information.

In quantum mechanics the destructive interference of wave functions in the presence of disorder may completely suppress diffusion, leading to the celebrated Anderson localization (AL) [1]. AL is driven by a competition between the disorder potential and the kinetic energy, and strongly depends on the spatial dimension [2]. The Anderson transition (AT) between metallic and localized phases in disordered systems presents an intriguing example of ergodicity breaking in non-interacting system, and remains a subject of theoretical [3] and experimental studies [4].

The search for delocalization transitions in one-dimensional systems with uncorrelated disorder motivated the introduction of models with power-law hoppings. In particular, the power-law banded matrices [5] became a prime example allowing for a detailed study of AT criticality. Further, random-matrix-type models without any spatial structure were recently considered [6]. The power-law banded matrices can be viewed as a one-dimensional system with a power-law hopping, $1/r^\sigma$, controlled by the exponent σ . Such system is localized when $\sigma > 1$, delocalized for $\sigma < 1$, and right at the AT for $\sigma = 1$.

In this work, we study a physical model, which realizes some of the phenomena observed in the power-law banded matrices. The key features of these toy models is the combination of long range hopping and disorder. Therefore, in order to mimic these Hamiltonians we consider the central site model (CSM) which consists of an Anderson localized fermionic chain, where all sites are coupled to an additional site (see inset in Fig. 1). While the fermionic chain without central site is Anderson localized for any non-zero disorder, the central site allows for hopping between arbitrary distant sites.

This model is motivated by central spin models [7–9] which adequately describe the hyperfine interaction between an electron spin captured in a quantum dot with the bath of nuclear spins in the host material [10, 11]. Central spin models are intrinsically interacting, and a

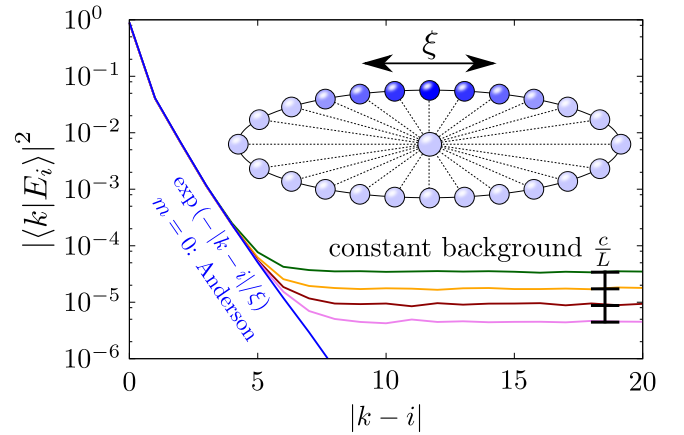


Figure 1. The wave function of the eigenstate that is localized on the site i initially decays exponentially with the distance $|k - i|$ with the same localization length as in the model without central site (blue line). Non-zero hopping to the central site, $m > 0$ leads to a saturation of the wave function amplitude to a constant background that scales as c/L . We show data for disorder strength $W = 10$, coupling strength $m = 1.25$ and $L \in \{2^9, 2^{10}, 2^{11}, 2^{12}\}$. The inset displays the schematic of the CSM, dashed lines represent the hopping terms m/\sqrt{L} .

possible realization of a localized phase with interactions — so called many-body localized (MBL) phase [12–14] — in such models is an intriguing open question. In this respect, the CSM model considered here is a natural simplification of central spin models to the non-interacting case. We will see that, despite being non-interacting, the CSM exemplifies exciting physical properties.

The CSM resembles the physics of the Fano resonance, where a single bound state is coupled to a continuum of energy levels [15]. There, a particle placed on the bound state is always vanishing in the continuum, because no localized eigenstates exist. In the CSM the continuum is replaced by an Anderson insulator that initially shows a Poisson distribution of level spacings. Consequently, we

find different regimes in the CSM depending on the value of coupling strength.

At weak couplings, the CSM retains a Poisson level statistic in most parts of the spectrum. In what follows we demonstrate that resonances in this part of the spectrum lead to logarithmic in time growth of entanglement entropy – a feature that is usually attributed as a hallmark of the interacting many-body localized phase [16–18]. As we increase the coupling constant to the central site, the system continuously evolves into a regime where it can be described within the Fano resonance framework. Here the level repulsion persists in the full spectrum, and the dynamics of entanglement is faster than logarithmic.

Model.— The CSM is described by the quadratic Hamiltonian $H = H_{\text{ring}} + H_c$ that consists of two parts. The first describes a one-dimensional disordered ring of size L , $H_{\text{ring}} = \sum_{i=1}^L h_i c_i^\dagger c_i + J (c_i^\dagger c_{i+1} + c_{i+1}^\dagger c_i)$, where c_i^\dagger and c_i are fermionic creation and annihilation operators. In H_{ring} , the on-site ring energies h_i are assumed to have random values uniformly distributed over the range $h_i \in [-W, W]$, where W quantifies the disorder strength and is assumed to be dominant over the hopping J , $W > J$.

The second part is referring to the Hamiltonian of the central site and its coupling to all ring sites,

$$H_c = \epsilon_0 c_0^\dagger c_0 + \frac{m}{\sqrt{L}} \sum_{i=1}^L c_i^\dagger c_0 + c_0^\dagger c_i, \quad (1)$$

where in what follows we set the energy of the central site, $\epsilon_0 = 0$, to be approximately in the middle of the localized band. Note, that we scale the coupling to the central site as $1/\sqrt{L}$, so that our system has a well defined thermodynamic limit. In the remainder of the paper we set $J = \hbar = 1$, and measure energy and time in units of J and \hbar/J , respectively.

Structure of eigenfunctions.— As already mentioned above, the coupling of the AL chain to the central site induces a partial delocalization of the Anderson peak. We can observe this in Fig. 1, where we show the average amplitude of the wave function $|E_i\rangle$ localized at site i as a function of distance from this site, $|k - i|$. We observe that the average probability of finding a particle along the system is still exponentially localized around the i th-site, with the AL length ξ [1, 2, 19] that is independent of m and coincides with the localization length of the Hamiltonian H_{ring} . Thus, the main effect of the coupling to the central site is a small, on average homogenous, background, which scales inversely proportional with the system size, i.e. like c/L [20]. Note that since the constant background scales as c/L and $\xi \ll L$, c can be naturally interpreted as the probability to find the particle away from the localization center. Remarkably, we observe this behavior for any value of m and not just in the limit of weak coupling to the central site.

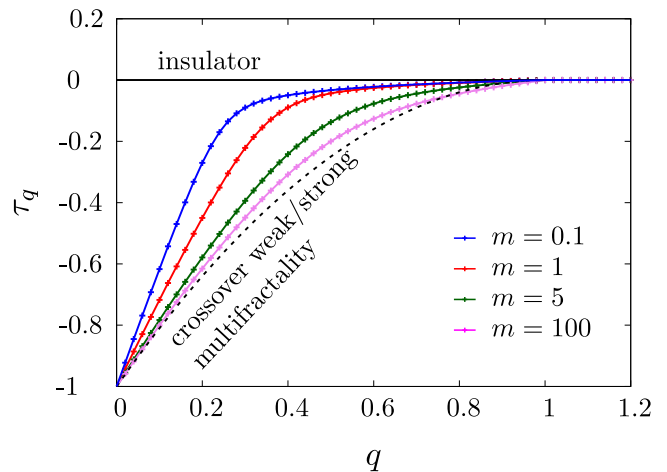


Figure 2. The spectrum of fractal dimension of participation ratios, τ_q , behaves in a qualitatively similar way for all values of coupling m . The convergence to $\tau_q = 0$ when $q \geq 1$ indicates a “frozen” fractal spectrum. For $m \ll W$, τ_q converges faster. Instead, for $m \gg W$, the fractal spectrum approaches $\tau_q = (1 - \gamma q)(q - 1)$ with $\gamma = 1$, suggesting a behavior intermediate between strong and weak multifractality [21]. Data is for eigenstates of the energy interval $\mathcal{I} = [2, 4]$ for disorder strength $W = 10$ and systems with up to $L = 2^{13}$ sites.

The constant background in Fig. 1 results from the averaging over individual eigenstates $|E_i\rangle$ for different disorder configurations. Separately, each wave function exhibits strong multifractal fluctuations [22]. We characterize these fluctuations by means of the moments of the participation ratios,

$$P_q = \langle \sum_k |\langle k | E_i \rangle|^2 \rangle_i \sim L^{-\tau_q}, \quad (2)$$

which we average over all eigenstates $|E_i\rangle$ and over disorder realizations. The scaling $P_q \sim L^{-\tau_q}$ defines $\tau_q = D_q(q - 1)$ and the fractal dimension D_q [22]. For the case of ideal metals or insulators, one expects the constant values $D_q = d$ and $D_q = 0$, respectively, where d is the spatial dimension. Instead, multifractal wave functions exhibit a dependency on q .

Fig. 2 demonstrates that the coupling to the central site partially destroys the insulating phase and gives rise to a non-trivial spectrum τ_q . Nevertheless, for all values of m we find $\tau_q = 0$ for $q \geq 1$. The convergence to $\tau_q = 0$ for $q \geq 1$ is called “frozen” fractal spectrum. This observation is consistent with the presence of the AL peak in Fig. 1, because for $q \sim 1$, all participation ratios are dominated by the largest values of the wave function.

For $q \ll 1$ instead, τ_q gives information about the distribution of the wave function outside of the AL peak. The multifractal fluctuations of the wave functions reveal themselves in the deviation from the metallic spectrum $\tau_q^{\text{metal}} = d(q - 1)$, which we would find for a constant

background. When $m \gg W$, the fractal dimension approaches $\tau_q = (1 - \gamma q)(q - 1)$ with $\gamma = 1$ (see dashed line in Fig. 2). This behavior suggests a phase in between strong and weak multifractality [21]. For $m \ll W$ in contrast, τ_q , and especially its slope at $q = 0$, depend on m .

Level statistics.— The existence of two different regimes, depending on the value of the coupling m can be understood by studying the influence of coupling to the central site on the level statistics, which is Poissonian in its absence. Perturbatively, an eigenstate with energy ϵ will acquire a correction $m^2/(\epsilon L)$. Comparing this shift to the mean level spacing $\delta = 2W/L$, we define the crossover energy ϵ_* , where $m^2/(\epsilon L) \sim \delta$. Hence, only the energy levels within $[-\epsilon_*, \epsilon_*]$ acquire level repulsion. At weak coupling strengths $m \ll W$, this interval is negligible and Poisson statistics dominates. It is this feature that breaks the applicability of the conventional Fano resonance picture, which relies on the presence of level repulsion [15].

We verify the existence of the interval $[-\epsilon_*, \epsilon_*]$ in Fig. 3, where we study eigenvalues within the energy window $\mathcal{I} = [2, 4]$. At $m \ll W$, eigenstates within \mathcal{I} are weakly perturbed and we observe the Poisson statistics of level spacings. For larger values of m , the interval of perturbed eigenvalues overlaps with \mathcal{I} , giving rise to a decrease of $P(s)$ for $s \rightarrow 0$ in Fig. 3. For $m \gtrsim W$, the interval $[-\epsilon_*, \epsilon_*]$ covers the whole band and thus, the entire spectrum shows level repulsion. Nevertheless, the level statistics is not described by a Wigner-Dyson distribution, as the $P(s)$ retains exponential tails. The slow decay of probability to have large level spacing (simple exponential, rather than Gaussian) suggests the finite level compressibility. This is natural: while a single central site can easily split degeneracies causing the level repulsion at small s , it cannot lead to a strong mixing of eigenstates with very different energies. Hence the fluctuations in the level spacing between k -th nearest neighbor eigenstates would grow proportionally to k , corresponding to finite compressibility. In this sense, the level statistics is closer to the critical level statistics seen at the AT [21].

Dynamics and entanglement growth.— Next we demonstrate how the energy scale ϵ_* affects the dynamical properties of the model. To this end, we study the spreading of information, witnessed by entanglement growth, which can in our noninteracting model only occur due to particle transport. The entanglement growth is thus strongly correlated with the motion of the particles. We consider the time evolution of the entanglement entropy $S_A(t)$ [23–25] which is frequently analyzed to identify the localization transition (with and without interactions). Using an equal size bipartition A, B of the Hilbert space \mathcal{H} in real space, we quantify the correlations among them by studying the von Neumann entropy $S_A(t)$ of the reduced density matrix. The evolution

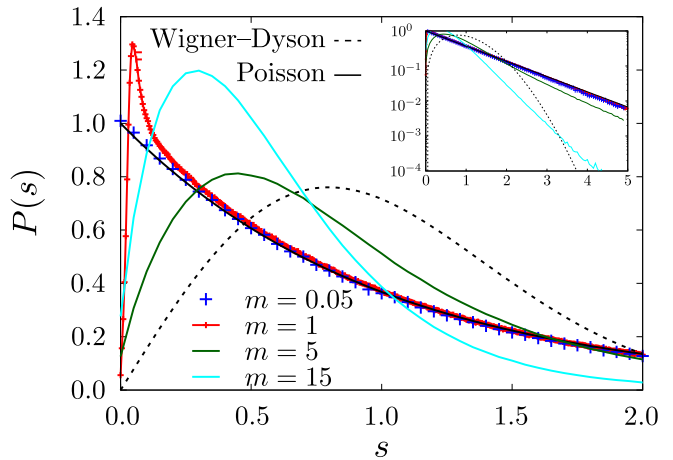


Figure 3. Density of the probability $P(s)$ of level spacings $s = (E_i - E_{i-1})/\delta$ between adjacent energy levels E_i and E_{i-1} in the energy range $E_i \in [2, 4]$ for $W = 10$ and $L = 2^{10}$. The level repulsion develops in the distribution of the level spacings upon increasing values of the coupling to the central site. The tails of the distributions always remain Poisson-like, as is revealed by their exponential decay shown in the inset.

of $S_A(t)$ provides then a direct measure of the spread of information throughout the system. In noninteracting systems, $S_A(t)$ can be written in terms of the correlation matrix $C_{ij}^A = \langle \psi(t) | c_i^\dagger c_j | \psi(t) \rangle$ [26, 27], with $i, j \in A$, as

$$S_A(t) = -\text{tr}[C^A \ln C^A + (1 - C^A) \ln(1 - C^A)]. \quad (3)$$

In Fig. 4, we show the time evolution of $S_A(t)$ in the three regimes of the coupling strength. As expected for $m = 0$ we recover the AL phase, characterized by a quick saturation of $S_A(t)$ to a value independent of L . Also, when $m \gtrsim W$, the resulting $S_A(t)$ exhibits a typical linear time-dependence [23, 28]. However, in the case of non-zero but small $m \ll W$, we find a logarithmic dependence of $S_A(t)$ on time, which lies in between both phases. The saturation value of $S_A(t)$ scales linearly with the system size for any $m > 0$ [20]. As mentioned above, the logarithmic growth of entanglement has been associated so far to many-body localized phases where information spreads via interactions between the particles [17, 18]. To the best of our knowledge, the logarithmic growth together with a saturation value that scales linearly with system size has never been observed in a non-MBL system before. Recently, a similar situation in the absence of interactions but without a linear scaling with system size has been identified in a different model [29].

In order to understand the entanglement dynamics, we study how particles move through the central site that connects any possible bipartition. Thus, we consider how a particle placed at a specific site on the ring evolves with the CSM Hamiltonian. Let us assume that this initial site has the strongest overlap with the eigenstate of energy ϵ of the unperturbed chain. The slowest dynamics is

generated by the mixing with almost degenerate energy levels. The coupling between these neighbored levels is according to perturbation theory $J_{nn} \sim m^2/(\epsilon L)$. Hence, the particle leaks into such an eigenstate on the timescale $t(\epsilon) \sim \epsilon L/m^2$. Eigenstates with $\epsilon > \epsilon_*$ are hardly perturbed by the central site. However, in rare cases with probability J_{nn}/δ , adjacent eigenstates are close to each other and strongly mixed by the central site. Then, the particle is equally likely to be found in both eigenstates at large times, contributing to a probability that the particle left its initial eigenstate given by $\bar{n}_\epsilon \sim J_{nn}/\delta \sim m^2/(W\epsilon)$.

The above intuition can be quantified by a three-site model. Within this toy-model, we study the motion of a particle starting on a site of potential ϵ through the central site into the continuum. When the coupling to the central site is weak, $m \ll W$, we are in the perturbative regime where mixing occurs with a small number of sites within $[-\epsilon_*, \epsilon_*]$. Hence in our case it suffices to consider the coupling to a single site of energy ϵ' and average over all $\epsilon' \in [-W, W]$ after the equations of motions are solved. This average neglects correlations between initially unoccupied ring sites, which is a reasonable assumption for $m \ll W$. However, it accounts for a small level splitting which, in contrast to the conventional Fano resonance [15], is present in our problem due to the Poisson distribution of level spacings in the unperturbed model. Using the three-site model [20], the probability $n_\epsilon(t)$ that the particle left its initial site becomes

$$n_\epsilon(t) \approx \begin{cases} \frac{\pi m^4}{WL} \left(\frac{t}{\epsilon^2}\right), & \frac{\sqrt{6}}{\epsilon} \leq t \leq \frac{\epsilon L}{4m^2}, \\ \bar{n}_\epsilon = \frac{\pi m^2}{4W} \left(\frac{1}{\epsilon}\right), & t \geq \frac{L\epsilon}{4m^2}, \end{cases} \quad (4)$$

which depends on the potential at the initial position. At a given time t , sites with energy $\epsilon < \epsilon_t = 4m^2 t/L$ have saturated their dynamics. Summing the contributions from all such sites, we get that the number of particles that are located at other sites is

$$n(t) = \frac{1}{2W} \int_{-\epsilon_t}^{\epsilon_t} n_\epsilon(t) d\epsilon = \frac{\pi m^2}{4W^2} \ln\left(\frac{m^2}{L} t\right) + \dots, \quad (5)$$

where ellipses denote possible constant terms. The logarithmic dependence here emerges from the summation over all possible energies of initial site, which translates into the integral of $1/\epsilon$ over ϵ with limits set by time. In the inset of Fig. 4 we compare the result of the three-site model, Eq. (5), with the numerical data of the full model and find good agreement in the regime of logarithmic growth of entanglement. As we outline in [20], the entanglement entropy $S_A(t)$ can be expressed by means of $n_\epsilon(t)$, which explains the logarithmic time-dependence of the entanglement entropy, plotted in Fig. 4.

Finally, at $m \geq W$, the energy scale ϵ_* becomes of the order of the bandwidth W . Consequently, level repulsion is present for all energy states of the Hamiltonian. Then, we expect much faster spreading of the particles, caused by the strong level admixture: the saturation time in

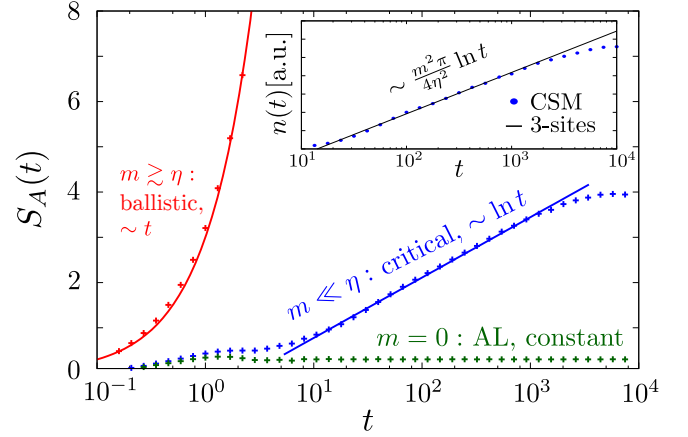


Figure 4. Entanglement growth of the initial product state with $L/2$ fermions, where every other site is occupied, $|0101\dots 01\rangle$. Upon changing the value of m , we observe Anderson insulating behavior ($m = 0$, central site is decoupled), a regime of logarithmic entanglement growth ($W \gg m > 0$), and eventually a polynomial in time entanglement dynamics for $m \geq W$. The data is for $L = 512$ ring sites, disorder strength $W = 10$, and coupling $m = 0$ (green), $m = 1$ (blue), and $m = 10$ (red). The inset illustrates that numerical results for the number of particles that changed their bipartition agree with analytical predictions for $m = 1$.

such regime becomes simply an inverse level spacing $1/\delta$. Inserting this into the first line of Eq. (4), we get $\bar{n}_\epsilon \propto 1/\epsilon^2$. Averaging this over the initial energy ϵ results in the linear spreading of $n(t)$, and ballistic entanglement dynamics, as confirmed in Fig. 4.

Summary— We have considered the behavior of an Anderson localized fermionic chain perturbed by coupling all sites to the additional central site. The eigenstates after perturbation lose their local character, but still keep the localized statistics. Statistics of level spacings and dynamical probes reveal the crossover between two different regimes. In the weak coupling regime, most of the eigenvalues of the system are Poisson-distributed, which leads to a break down of the Fano resonance picture. This regime shows logarithmic in time growth of entanglement entropy caused by the spreading of particles. The second regime, where level repulsion is present, can be mapped to the Fano resonance problem, and it is characterized by ballistic motion of entanglement.

Overall our findings support the intuition that a single degree of freedom, even if it is coupled non-locally to the Anderson insulator is not sufficient to delocalize the system. In addition, our results suggest that logarithmic entanglement growth can be realized in non-interacting models of free fermions, and is related to the persistence of the Poisson level statistics in parts of the spectrum.

Acknowledgments— We would like to thank Dmitry Abanin, Christophe De Beule, Joel Moore, Romain Vasseur, and Norman Yao for many stimulating discussions. Financial support has been provided by the

Deutsche Forschungsgemeinschaft (DFG). M.S. was supported by Gordon and Betty Moore Foundation's EPiQS Initiative through Grant GBMF4307. F. D. acknowledges financial support from the DFG via SFB 1170 "ToCoTronics" and the ENB Graduate School on Topological Insulators.

-
- [1] P. W. Anderson, "Absence of Diffusion in Certain Random Lattices," *Phys. Rev.* **109**, 1492–1505 (1958).
 - [2] B. Kramer and A. MacKinnon, "Localization: theory and experiment," *Reports Prog. Phys.* **56**, 1469 (1993).
 - [3] Ferdinand Evers and Alexander D Mirlin, "Anderson transitions," *Rev. Mod. Phys.* **80**, 1355–1417 (2008).
 - [4] J. Chabé, G. Lemarié, B. Grémaud, D. Delande, P. Szriftgiser, and J. C. Garreau, "Experimental Observation of the Anderson Metal-Insulator Transition with Atomic Matter Waves," *Phys. Rev. Lett.* **101**, 255702 (2008), [arXiv:0709.4320](#).
 - [5] A. D. Mirlin and F. Evers, "Multifractality and critical fluctuations at the Anderson transition," *Phys. Rev. B - Condens. Matter Mater. Phys.* **62**, 7920–7933 (2000), [arXiv:0003332 \[cond-mat\]](#).
 - [6] V. E. Kravtsov, I. M. Khaymovich, E. Cuevas, and M. Amini, "A random matrix model with localization and ergodic transitions," *New J. Phys.* **17**, 122002 (2015), [arXiv:1508.01714](#).
 - [7] Daniel Loss and David P. DiVincenzo, "Quantum computation with quantum dots," *Phys. Rev. A* **57**, 120–126 (1998), [arXiv:9701055 \[cond-mat\]](#).
 - [8] John Schliemann, Alexander V. Khaetskii, and Daniel Loss, "Spin decay and quantum parallelism," *Phys. Rev. B* **66**, 245303 (2002).
 - [9] Michael Bortz and Joachim Stolze, "Exact dynamics in the inhomogeneous central-spin model," *Phys. Rev. B* **76**, 014304 (2007), [arXiv:0612382 \[cond-mat\]](#).
 - [10] W. A. Coish and Daniel Loss, "Hyperfine interaction in a quantum dot: Non-Markovian electron spin dynamics," *Phys. Rev. B* **70**, 195340 (2004).
 - [11] Jan Fischer, Björn Trauzettel, and Daniel Loss, "Hyperfine interaction and electron-spin decoherence in graphene and carbon nanotube quantum dots," *Phys. Rev. B* **80**, 155401 (2009), [arXiv:0906.2800](#).
 - [12] Boris L. Altshuler, Yuval Gefen, Alex Kamenev, and Leonid S. Levitov, "Quasiparticle Lifetime in a Finite System: A Nonperturbative Approach," *Phys. Rev. Lett.* **78**, 2803–2806 (1997), [arXiv:9609132 \[cond-mat\]](#).
 - [13] I. V. Gornyi, A. D. Mirlin, and D. G. Polyakov, "Interacting electrons in disordered wires: Anderson localization and low-T transport," *Phys. Rev. Lett.* **95**, 1–4 (2005), [arXiv:0506411 \[cond-mat\]](#).
 - [14] D.M. Basko, I.L. Aleiner, and B.L. Altshuler, "Metal-insulator transition in a weakly interacting many-electron system with localized single-particle states," *Ann. Phys. (N. Y.)* **321**, 1126–1205 (2006), [arXiv:0506617 \[cond-mat\]](#).
 - [15] Gerald D. Mahan, *Many-Particle Physics*, 2nd ed. (Plenum Press, 1990).
 - [16] Marko Žnidarič, Tomaž Prosen, and Peter Prelovšek, "Many-body localization in the Heisenberg XXZ magnet in a random field," *Phys. Rev. B - Condens. Matter Mater. Phys.* **77**, 1–5 (2008), [arXiv:0706.2539](#).
 - [17] Jens H. Bardarson, Frank Pollmann, and Joel E. Moore, "Unbounded Growth of Entanglement in Models of Many-Body Localization," *Phys. Rev. Lett.* **109**, 017202 (2012), [arXiv:arXiv:1202.5532v2](#).
 - [18] Maksym Serbyn, Z. Papic, and Dmitry A. Abanin, "Universal slow growth of entanglement in interacting strongly disordered systems," *Phys. Rev. Lett.* **110** (2013), 10.1103/PhysRevLett.110.260601, [arXiv:1304.4605](#).
 - [19] T. Giamarchi and H. J. Schulz, "Anderson localization and interactions in one-dimensional metals," *Phys. Rev. B* **37**, 325–340 (1988).
 - [20] See supporting online material for more detailed discussions and derivations, .
 - [21] Alexander D. Mirlin, "Statistics of energy levels and eigenfunctions in disordered systems," *Phys. Rep.* **326**, 383 (2000).
 - [22] Michael Schreiber and Heiko Grussbach, "Multifractal wave functions at the Anderson transition," *Phys. Rev. Lett.* **67**, 607–610 (1991).
 - [23] Pasquale Calabrese and John Cardy, "Evolution of entanglement entropy in one-dimensional systems," *J. Stat. Mech. Theory Exp.* **2005**, P04010 (2005), [arXiv:0503393 \[cond-mat\]](#).
 - [24] David J. Luitz, Nicolas Laflorencie, and Fabien Alet, "Many-body localization edge in the random-field Heisenberg chain," *Phys. Rev. B* **91**, 081103 (2015), [arXiv:1411.0660v2](#).
 - [25] A. M. Kaufman, M. E. Tai, A. Lukin, M. Rispoli, R. Schittko, P. M. Preiss, and M. Greiner, "Quantum thermalization through entanglement in an isolated many-body system," *Science* **353**, 794–800 (2016).
 - [26] Siew-Ann Cheong and Christopher L. Henley, "Many-body density matrices for free fermions," *Phys. Rev. B* **69**, 075111 (2004).
 - [27] Ingo Peschel, "Calculation of reduced density matrices from correlation functions," *J. Phys. A: Math. Gen.* **36**, 4 (2002), [arXiv:0212631 \[cond-mat\]](#).
 - [28] Elliott H. Lieb and Derek W. Robinson, "The finite group velocity of quantum spin systems," *Commun. Math. Phys.* **28**, 251–257 (1972).
 - [29] Rajeev Singh, Roderich Moessner, and Dibyendu Roy, "Effect of long-range hopping and interactions on entanglement dynamics and many-body localization," , 1–10 (2016), [arXiv:1606.04542](#).

SUPPLEMENTARY ONLINE MATERIAL

A. Mapping to Fano resonance problem

A.1. Spectral weight and position of the resonance

Physically, the CSM resembles the physics of the Fano resonance, when we have a single site coupled to a continuum. Then, there is a leading order self-energy correction, which determines the new position of the resonance,

$$\Sigma(i\omega) = \frac{m^2}{L} \sum_{\alpha} \frac{1}{i\omega - \varepsilon_{\alpha}}, \quad (\text{S1})$$

where ε_{α} labels energies of localized eigenstates. Approximating the sum with an integral, we deduce the following self-consistent equation for the new position of the resonance ω_r expressed via the dimensionless variable x as $\omega_r = Wx$:

$$x = \frac{m^2}{2W^2} \ln \frac{x-1}{x+1}. \quad (\text{S2})$$

On the one hand, when $m \gg W$, we expect that $x \gg 1$. Then, we can expand the log and get:

$$x = \frac{m}{\sqrt{2}W} \gg 1. \quad (\text{S3})$$

On the other hand, if the coupling is weak, we obtain $x - 1 \ll 1$, so we have a resonance which is very close to the band edge,

$$x - 1 = 2e^{-2W^2/m^2} \ll 1. \quad (\text{S4})$$

Depending on x , we can have a very different spectral weight on the resonance,

$$Z = [1 - \partial_{\omega} \text{Re} \Sigma(\omega_r)]^{-1} = \left(1 + \frac{m^2}{L\delta W} \frac{2}{x^2 - 1}\right)^{-1}. \quad (\text{S5})$$

For the strong coupling, when $x \gg 1$, we get:

$$Z \approx \frac{1}{2} \left(1 - \frac{1}{2x^2}\right), \quad (\text{S6})$$

so that the spectral weight is almost 1/2. In this case we get very small spectral weight in the bath that scales as $1/x^2 \propto W^2/m^2$. On the other hand, when $x \ll 1$, we have

$$Z \approx 2e^{-2W^2/m^2} \ll 1, \quad (\text{S7})$$

so that the spectral weight that remains in the continuum is close to one. However, in both cases, we recover that the spectral weight remaining in the bath does not scale with the system size.

Since the only way to get delocalized states arises from the hopping via the central site, we conclude that the constant weight, when distributed among L states in the continuum, will give a $\propto 1/L$ constant background of the wave function. The same result will be derived below from the three-site model.

A.2 Dynamics and breakdown of the Fano description

Using self-consistent perturbation theory, we can calculate the expansion of eigenstates with the central site over unperturbed eigenstates. This expansion reads [15]:

$$c_0 = \sum_i \nu_i \alpha_i, \quad c_i = \sum_j W_{ij} \alpha_j. \quad (\text{S8})$$

The coefficients W_{ij} are expressed via $Z_i = Z(\epsilon_i)$ as

$$W_{ij}^2 = \frac{A^2 \nu_j^2}{(\epsilon_i - \epsilon_j)^2} + \delta_{ij} \frac{Z_i^2}{Z_i^2 + (2\pi/\delta)^2}. \quad (\text{S9})$$

Note, that the self-energy in Eq. (S5) defining Z is given by:

$$\Sigma(\omega) = \frac{A^2}{\delta} \text{arctanh} \frac{\omega}{W} \quad \text{for } |\omega| < W. \quad (\text{S10})$$

Now, we are interested in the amplitude of the wave function, that is not located on the initial eigenstate with energy ϵ_i , which we denote as n_{ϵ} (index i is omitted for brevity). To calculate this amplitude, we sum:

$$\begin{aligned} n_{\epsilon} &= \sum_{j \neq i} |W_{ij}|^2 = \sum_{j \neq i} \frac{1}{(\epsilon_i - \epsilon_j)^2} \frac{1}{Z_j^2 + (2\pi/\delta)^2} \\ &= \frac{1}{\delta} \int d\omega \frac{1}{(\omega - \epsilon)^2} \frac{m^4/L^2}{[\omega - \Sigma(\omega)]^2 + (\pi m^2/W)^2}. \end{aligned} \quad (\text{S11})$$

To deduce the dependence on time, we can limit the sum in Eq. (S11) to states j with energy difference such that $|\epsilon - \epsilon_j| \geq 1/t$:

$$\begin{aligned} n_{\epsilon}(t) &= \sum_{j \neq i} |W_{ij}|^2 \\ &= \frac{2}{\delta} \int_{1/t}^{\infty} d\omega \frac{1}{\omega^2} \frac{m^4/L^2}{[\omega - \epsilon - \Sigma(\omega - \epsilon)]^2 + (\pi m^2/W)^2}. \end{aligned} \quad (\text{S12})$$

The integral yields the asymptotic expression

$$n_{\epsilon}(t) = \frac{1}{3} \frac{m^4}{LW} t^3 \quad (\text{S13})$$

at small times $t \ll 1/\epsilon_i$. For longer times, when $W/m^2 > t > 1/\epsilon$, assuming that $\epsilon > m^2/W = \epsilon_*$, we get:

$$n_{\epsilon}(t) \propto \frac{m^4}{WL} \frac{t}{\epsilon^2}, \quad (\text{S14})$$

the linear growth of particle density that is located away from initial eigenstate. Note, that for $t = 1/\delta$ this expression gives us the saturation value that can be directly obtained from Eq. (S11):

$$\bar{n}_{\epsilon} = n_{\epsilon}(1/\delta) = \frac{m^4}{4W^2} \frac{2}{\epsilon_i^2 + (\pi m^2/W)^2} \propto \frac{m^4}{W^2} \frac{1}{\epsilon_i^2}. \quad (\text{S15})$$

We see that \bar{n}_ϵ is suppressed as $1/\epsilon^2$ when the absolute value of energy is bigger than the crossover scale, $|\epsilon| > m^2/W = \epsilon_*$ defined in the main text. Such dependence would lead to a ballistic spreading of particles, and consequently a linear spreading of entanglement entropy.

In all above considerations, we however ignored the almost resonant pairs of sites. This is a legitimate assumption when the initial bath of states has level repulsion, so that the probability to have degenerate energies is vanishing. It is this assumption that breaks down for the present model, specifically outside the energy window $[-\epsilon_*, \epsilon_*]$. In order to rigorously consider the physics emerging from such resonances, in the next section we present a toy model which allows for an analytical understanding.

B. Beyond Fano picture: three-site model

B.1. Time dependent perturbation theory

In order to derive the logarithmic growth of entanglement entropy, we study the motion of single fermion below. In particular, we calculate $n_\epsilon(t)$ for small times perturbatively and compare our analytical results with numerical data for the central site model.

We have found out that it is important to treat the coupling between initial site and central site exactly. This is because the two hybridized states, a mixture of the initial site and the central site, contain the essential physics how the excitation moves into the remainder of the system. Thus, we consider the following, unperturbed Hamiltonian

$$H_0 = \epsilon c_1^\dagger c_1 + A c_1^\dagger c_0 + A c_0^\dagger c_1 + \sum_{i \geq 2} h_i c_i^\dagger c_i, \quad (\text{S16})$$

where A is the coupling to the central site, and in the main text we used $A = m/\sqrt{L}$. If we diagonalize this Hamiltonian, we obtain

$$H_0 = \lambda_+ f_0^\dagger f_0 + \lambda_- f_1^\dagger f_1 + \sum_{i \geq 2} h_i c_i^\dagger c_i \quad (\text{S17})$$

with $\lambda_\pm = \frac{\epsilon}{2} \pm \sqrt{A^2 + \frac{\epsilon^2}{4}}$. Within this basis, the (per-

turbatively treated) coupling term becomes

$$V := \sum_{i \geq 2} (c_i^\dagger c_0 + c_0^\dagger c_i) \quad (\text{S18})$$

$$= n_- \sum_{i \geq 2} (f_i^\dagger f_1 + f_1^\dagger f_i) + n_+ \sum_{i \geq 2} (f_i^\dagger f_0 + f_0^\dagger f_i) \quad (\text{S19})$$

and the initial state can be written as

$$|\psi(t=0)\rangle = c_1^\dagger |\emptyset\rangle = \frac{1}{A} (n_+ \lambda_+ f_0^\dagger + n_- \lambda_- f_1^\dagger) |\emptyset\rangle \quad (\text{S20})$$

with $n_\pm = 1/\sqrt{1 + \lambda_\pm^2/A^2}$ and $|\emptyset\rangle$ is the (empty) vacuum state. The total Hamiltonian is then given by $H = H_0 + AV$ and we are interested in the probability $|\langle n | \psi(t) \rangle|^2$ to find the Fermion on another ring site $n \geq 2$ with potential $h_n \in [-W, W]$. To solve this problem, we use the Ansatz

$$|\psi(t)\rangle = \sum_n b_n(t) \exp(-ih_n t) |\phi_n\rangle, \quad (\text{S21})$$

where $|\phi_n\rangle = c_n |\emptyset\rangle$ for $n \geq 2$ and $|\phi_n\rangle = f_n |\emptyset\rangle$ for $n \in \{0, 1\}$ are the eigenstates of H_0 . Inserting $|\psi(t=0)\rangle$ in the Schrödinger equation, this yields

$$i \frac{d}{dt} b_n(t) = \sum_k e^{i(h_n - h_k)t} V_{nk} b_k(t), \quad (\text{S22})$$

where $h_i = \lambda_\pm$ for $i \in \{0, 1\}$ and $V_{nk} = \langle \phi_n | V | \phi_k \rangle$. This exact solution is now approximated by the expansion (in powers of A)

$$b_n(t) = b_n^{(0)}(t) + A b_n^{(1)}(t) + A^2 b_n^{(2)}(t) + \dots, \quad (\text{S23})$$

for which we find

$$i \frac{d}{dt} b_n^{(r)}(t) = \sum_k e^{i(h_n - h_k)t} V_{nk} b_k^{(r-1)} \quad r \geq 1 \quad (\text{S24})$$

$$i \frac{d}{dt} b_n^{(0)}(t) = 0. \quad (\text{S25})$$

Using the initial conditions (see Eq. (S20)) $b_0^{(0)}(t=0) = n_+ \lambda_+ / A$, $b_1^{(0)}(t=0) = n_- \lambda_- / A$, and $b_n^{(0)}(t=0) = 0$ for all $n \geq 2$, this implies

$$i \frac{d}{dt} b_n^{(1)}(t) = \frac{1}{A} \left(\lambda_+ n_+^2 e^{i(h_n - \lambda_+)t} + \lambda_- n_-^2 e^{i(h_n - \lambda_-)t} \right) \quad (\text{S26})$$

and

$$i \frac{d}{dt} b_n^{(2)}(t) = \sum_{k \in \{0,1\}} e^{i(h_n - h_k)t} V_{nk} \underbrace{b_k^{(1)}(t)}_{=0} = 0. \quad (\text{S27})$$

The time dependent probability that the Fermion is present at site $n \geq 2$ is then well approximated by

$$\begin{aligned}
n_\epsilon(t, h_n) &:= |\langle \phi_n | \psi(t) \rangle|^2 \approx \left| b_n^{(0)} + A b_n^{(1)}(t) + A^2 b_n^{(2)} \right|^2 \\
&= \frac{2n_+^4 \lambda_+^2 [1 - \cos(h_n - \lambda_+ t)]}{(h_n - \lambda_+)^2} + \frac{2n_-^4 \lambda_-^2 [1 - \cos(h_n - \lambda_- t)]}{(h_n - \lambda_-)^2} \\
&\quad + \frac{2n_-^2 n_+^2 \lambda_- \lambda_+ \{1 - \cos[(h_n - \lambda_+)t] - \cos[(h_n - \lambda_-)t] + \cos[(\lambda_- - \lambda_+)t]\}}{(h_n - \lambda_+)(h_n - \lambda_-)}
\end{aligned} \tag{S28}$$

With this result at hand, we sum the contributions of all L sites with random potential h_n . In the numerical simulation, this is automatically done by considering many independent Fermions at a time and by averaging over disorder. Mathematically, we do this by

$$n_\epsilon(t) = \frac{L}{2W} \int_{-W}^W dh n_\epsilon(t, h). \tag{S29}$$

Using the principal value of the integral and extending the integration boundaries to $(-\infty, \infty)$, which corresponds to a small mistake for $A \ll W$, the integral becomes

$$n_\epsilon(t) \approx \frac{L}{2W} \frac{4A^4 \pi}{\Delta^3} (t\Delta - \sin(t\Delta)), \tag{S30}$$

where $\Delta = 2\sqrt{A^2 + \frac{\epsilon^2}{4}}$ is the level splitting. For times $t \gg \frac{1}{\Delta}$, we hence have derived the linear growth of $n_\epsilon(t)$. For times $t \ll \frac{1}{\Delta}$, we find an initial cubic growth of $n_\epsilon(t)$, which coincides with Eq. (S13), but is not important for the logarithmic growth of entanglement entropy. In Fig. S1, we compare the perturbation theories with exact numerics and find good agreement.

B.2. Saturation values

In this section, we specify the limit

$$\bar{n}_\epsilon := \lim_{T \rightarrow \infty} \frac{1}{T} \int_0^T dt n_\epsilon(t). \tag{S31}$$

Recall that $n_\epsilon(t) = \sum_{i \geq 2}^N \langle \psi(t) | c_i^\dagger c_i | \psi(t) \rangle$ is the probability that the single fermion left its initial site and is now present in the bath. In order to derive $\bar{n}_\epsilon(t)$, we first resolve it by energy, i.e.

$$\bar{n}_\epsilon(E) dE = \sum_{\substack{i \geq 2 \\ E \leq h_i < E+dE}}^N \lim_{T \rightarrow \infty} \frac{1}{T} \int_0^T dt \langle \psi(t) | c_i^\dagger c_i | \psi(t) \rangle. \tag{S32}$$

As in the previous chapter, we treat the initial site $i = 1$ and the central site $i = 0$ exactly, i. e. we diagonalize their two-site Hamiltonian $H_0 = 0c_0^\dagger c_0 + \epsilon c_1^\dagger c_1 + A(c_1^\dagger c_0 +$

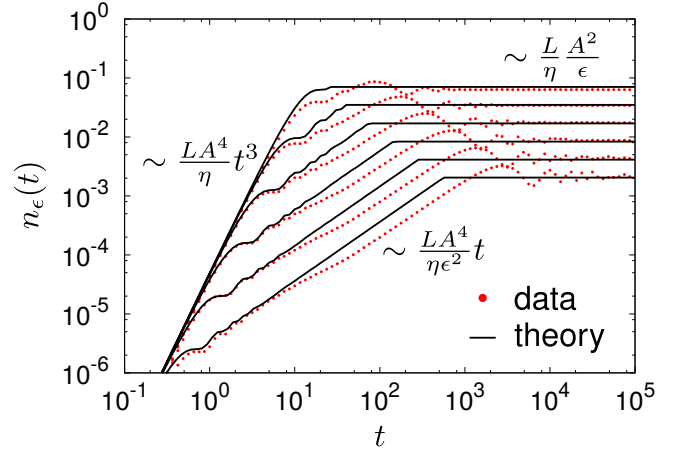


Figure S1. The probability $n_\epsilon(t)$, that a Fermion, initially placed at a site of potential ϵ , left its site and is located at another ring site has different behavior depending on the value of ϵ . Upon increasing $\epsilon \in \{0.4, 0.8, 1.6, 3.2, 6.4\}$ from top to bottom, we see that the time interval where $n_\epsilon(t)$ has a linear in time growth increases, while the saturation value decreases.

$c_0^\dagger c_1$) and find the two hybridized states f_0 and f_1 . Subsequently, we couple these two states independently to a single bath state of energy E .

In a simple two site problems with energy gap Δ_{if} and coupling constant A , the probability to find an excitation outside its initial position is (averaged over time) given by

$$\bar{P}_{if} = \frac{2A^2}{\Delta_{if}^2 + 4A^2}. \tag{S33}$$

The probability we seek is thus well approximated by

$$\begin{aligned}
\bar{n}_\epsilon(h_i) &= |\langle f_0 | \psi_0 \rangle|^2 \bar{P}_{f_0 i} + |\langle f_1 | \psi_0 \rangle|^2 \bar{P}_{f_1 i} \\
&= \frac{\lambda_+^2 n_+^2}{A^2} \frac{2n_+^2 A^2}{(\lambda_+ - h_i)^2 + 4A^2 n_+^2} \\
&\quad + \frac{\lambda_-^2 n_-^2}{A^2} \frac{2n_-^2 A^2}{(\lambda_- - h_i)^2 + 4A^2 n_-^2}.
\end{aligned} \tag{S34}$$

This probability is derived for one single bath state. We actually have $L - 1$ bath states uniformly distributed in the energy window $[-W, W]$, resulting in a level density of $\frac{L-1}{2W}$. The average effect of all $L - 1$ bath sites is

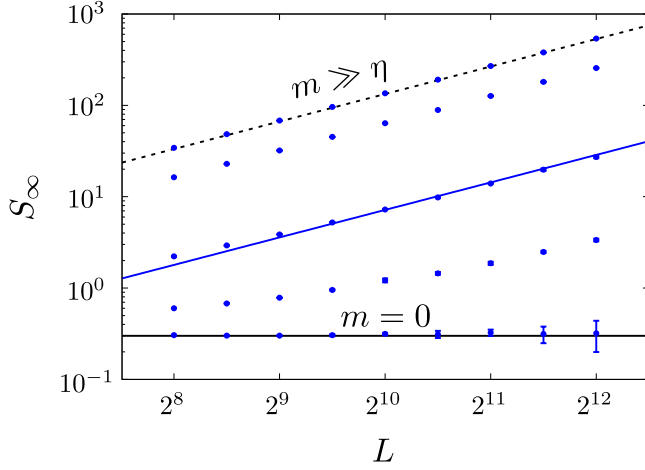


Figure S2. Saturation value of the entanglement entropy $S_\infty = \lim_{t \rightarrow \infty} S(t)$ for different system sizes L and coupling values $m \in \{0, 0.25, 1, 5, 20\}$ (bottom to top) and $W = 10$. For all coupling constants $m > 0$ we find a linear scaling $S_\infty \sim L$, e.g. we compare the data set of $m = 1$ with $S_\infty = 0.007L$ (blue line). This feature, together with the logarithmic in time growth of $S(t)$ (see Fig. 4) has never been observed before in a noninteracting system.

thus given by

$$\bar{n}_\epsilon = \int_{-\infty}^{\infty} dh \frac{L-1}{2W} \bar{n}_\epsilon(h) = \frac{L-1}{2W} \frac{\pi}{A} [\lambda_+^2 n_+^3 + \lambda_-^2 n_-^3] \quad (S35)$$

$$\stackrel{A \ll \epsilon}{\approx} \frac{L-1}{2W} \frac{A^2 \pi}{\epsilon} + \mathcal{O}(A^3)$$

Here, we are weakly overestimating the probability \bar{n}_ϵ due to two reasons. First, the integral should be taken from $-W$ to W . However, as we explicitly checked, the error caused by extension of integration limits to infinity is negligible for small $A \ll \epsilon < W$. Secondly, although the assumption that all bath states are uncoupled is valid for small A , it underestimates the physical outcome. In the numerical simulation, the particle has more than one possibility to enter the ring sites. The “fraction” of the particle that goes to an E_1 ring site can no longer go to an E_2 ring site and vice versa. Thus, the analytical theory, which assumes only one bath state at a time, is overestimating the probability \bar{n}_ϵ . In Fig. S1, we compare the derived saturation value with the numerical gained data and find perfect agreement in the regime $A \ll \epsilon$ (lower curves).

Eq. (S35) is not only completing the derivation of the logarithmic motion, but it also shows that saturation values should grow linear with system size. Indeed, we find that also the entanglement entropy saturates at values that grow linear with system size, see Fig. S2.

B.3. Constant background level

Previously, we have described that all eigenstates $|E_l\rangle$ of the full Hamiltonian are localized at a site l . On sites k far away from l , we see on average a constant probability $|\langle k|E_l\rangle|^2$ that the excitation $|E_l\rangle$ is measured at site k . With the above presented toy model, it is possible to deduce the correct scaling behavior of $|\langle k|E_l\rangle|^2 \sim \frac{m^2}{LW^2}$, which will be outlined next.

Let us consider again a single Fermion, initially placed at site k with potential ϵ . The time-averaged density matrix

$$\omega = \lim_{T \rightarrow \infty} \frac{1}{T} \int_0^T dt \rho(t) = \sum_l (\rho_0^E)_{ll} |E_l\rangle \langle E_l| \quad (S36)$$

with $\bar{n}_\epsilon(E_l) \equiv (\rho_0^E)_{ll} := |\langle E_l|\psi(t=0)\rangle|^2 = |\langle E_l|k\rangle|^2$ contains the probability $\bar{n}_\epsilon(E_l)$ to measure the initial excitation at long times with an energy E_l , which is the overlap $|\langle k|E_l\rangle|^2$ we search for. Before, we have been interested in the total probability that the initial excitation is somewhere in the bath and found

$$\bar{n}_\epsilon = \int_{-\infty}^{\infty} dh \frac{L-1}{2W} \bar{n}_\epsilon(h). \quad (S37)$$

Now, we want the *average* value of $|\langle E_l|k\rangle|^2 = \langle \bar{n}_\epsilon(E) \rangle_E$, which is for $L-1$ bath states consequently given by

$$\langle |\langle E_l|k\rangle|^2 \rangle_l = \frac{1}{L-1} \int_{-\infty}^{\infty} dh \frac{L-1}{2W} \bar{n}_\epsilon(h) = \frac{A^2 \pi}{2W\epsilon} \quad (S38)$$

Finally, we have to average over the potential ϵ of the initial site k , which gives

$$\langle |\langle E_l|k\rangle|^2 \rangle_{l,k} \approx 2 \frac{1}{2W} \int_{\alpha>0}^W d\epsilon \frac{A^2 \pi}{2W\epsilon} = \frac{A^2 \pi}{2W^2} \ln \frac{W}{\alpha}. \quad (S39)$$

In the main text of the Letter, we used $A = \frac{m}{\sqrt{L}}$ and found the constant background level $\sim \frac{m^2}{LW^2}$, which coincides with this result, as the logarithmic contribution of the disorder W is weak compared to the quadratic dependency and cannot be distinguished numerically.

C. Relation between entanglement entropy and particle transport

The entanglement entropy between two bipartitions A and B of a Hilbert space \mathcal{H} is usually measured by means of the von Neumann entropy of the reduced density matrix $\rho_A = \text{tr}_B[\rho(t)]$, i.e.

$$S_A(t) = -\text{tr}[\rho_A \ln \rho_A], \quad (S40)$$

where $\rho(t)$ describes the state of the system. For pure states $\rho = |\psi(t)\rangle \langle \psi(t)|$, $S_A(t) = S_B(t)$ for all t and bipartitions A, B , which can easily be shown using the Schmidt decomposition $|\psi\rangle = \sum_i \sqrt{\lambda_i} |i\rangle_A \otimes |i\rangle_B$.

For lattice systems of L sites and free Fermions, it is useful to describe a quantum state not with a vector $|\psi\rangle \in \mathcal{H} = \mathbb{C}^{2^L}$, but by the correlation matrix

$$C_{ij}(t) = \langle \psi(t) | c_i^\dagger c_j | \psi(t) \rangle \quad (\text{S41})$$

where c_i is a annihilation operator on site i , and thus, C is a correlation matrix of size $L \times L$ only. The matrix C contains all information about the full state $|\psi\rangle$ or ρ , because according to Wick's theorem any correlation function splits for independent Fermions into products of two-point correlators C_{ij} . Hence, also the entanglement entropy $S_A(t)$ is expressible by means of C , which is

$$S_A(t) = -\text{tr}[C_A \ln C_A + (\mathbb{1} - C_A) \ln(\mathbb{1} - C_A)], \quad (\text{S42})$$

and C_A is the part of C_{ij} with $i, j \in A$. As the Fermions are independent from each other, it is sufficient to consider a single fermion. The entanglement entropy is additive for independent degrees of freedom, hence, the total entanglement entropy sums up to $S_A(t) = \sum_i S_A^i(t)$, where $S_A^i(t)$ is the contribution of the i th Fermion. If only one fermion exists (in a pure state), the matrix C has only one nonzero eigenvalue, which is equal to unity. Hence, C is of rank 1 and all possible submatrices C_A are at maximum of rank 1 as well. For any bipartition A, B , the matrix C_A has at maximum one nonzero eigenvalue

λ , which equals for the same reason $\lambda = \text{tr}[C_A]$. The entanglement entropy thus simplifies to

$$S_A(t) = -\lambda \ln \lambda - (1 - \lambda) \ln(1 - \lambda). \quad (\text{S43})$$

Using the relation $\lambda = \text{tr}[C_A]$, we find

$$\lambda = \sum_{i \in A} \langle \psi(t) | c_i^\dagger c_i | \psi(t) \rangle = \sum_{i \in A} |\langle i | \psi \rangle|^2 = n_\epsilon(t) \quad (\text{S44})$$

where $n_\epsilon(t)$ is the probability, that the single fermion is present in the subspace A .

In the paper, $n_\epsilon(t)$ is the probability, that a single fermion, initially placed at a site of potential ϵ changed its bipartition at time t . Hence, we do have access to the entanglement entropy by

$$S_A(n_\epsilon(t)) = -n_\epsilon(t) \ln n_\epsilon(t) - (1 - n_\epsilon(t)) \ln(1 - n_\epsilon(t)). \quad (\text{S45})$$

By this equation, we have identified a direct connection between $n_\epsilon(t)$ analytically derived in Eq. (4) and the time evolution of the entanglement entropy $S_A(t)$. The ϵ -averaged expression for $n_\epsilon(t)$ explains the logarithmic spread of a particle in the CSM, see Eq. (5). Thus, the leading terms at intermediate time scales for the time evolution of $S_A(t)$ (which also shows a logarithmic time dependence) is directly related to this peculiar particle motion.